Effective subgrid-scale models for high-resolution LES

Andrew W. Cook

With some approximation, the large-eddy equations for flows comprised of N ideal gases can be written:

$$\dot{\rho}_\alpha + \nabla \cdot (\rho_\alpha \mathbf{u} + \mathbf{J}_\alpha) = 0 \ , \quad \alpha = 1, 2, ..., N \ , \tag{1}$$

$$\dot{\mathbf{m}} + \nabla \cdot (\rho \mathbf{u}\mathbf{u} + p\underline{\boldsymbol{\delta}} - \underline{\boldsymbol{\tau}}) = \rho \mathbf{g} \ , \tag{2}$$

$$\dot{E} + \nabla \cdot (E\mathbf{u} + p\underline{\boldsymbol{\delta}} \cdot \mathbf{u} - \underline{\boldsymbol{\tau}} \cdot \mathbf{u} + \mathbf{q}) = \mathbf{m} \cdot \mathbf{g} \ , \tag{3}$$

$$p = \rho \left(Y_\alpha H_\alpha - e\right) \ , \quad H_\alpha = \int_{T_o}^{T} c_{p,\alpha}(\mathcal{T})\, d\mathcal{T} \ , \quad T = \frac{p}{\rho R} \ , \quad R = R_o \sum_{\alpha=1}^{N} \frac{Y_\alpha}{M_\alpha} \ , \tag{4}$$

where $\mathbf{J}_\alpha$ is a subgrid-scale (sgs) mass flux vector, $\underline{\boldsymbol{\tau}}$ is the sgs stress tensor and $\mathbf{q}$ is the sgs heat flux vector. These subgrid terms can be modeled by analogy to the Navier-Stokes equations, i.e.,

$$\mathbf{J}_\alpha = -\rho D_\alpha \nabla Y_\alpha \quad (\text{no sum on } \alpha) \ , \tag{5}$$

$$\underline{\boldsymbol{\tau}} = \mu[\nabla \mathbf{u} + (\nabla \mathbf{u})^\dagger] + (\mu_b - \frac{2}{3}\mu)(\nabla \cdot \mathbf{u})\underline{\boldsymbol{\delta}} \ , \tag{6}$$

$$\mathbf{q} = -k \nabla T \ , \tag{7}$$

where D_α, μ, μ_b and k are grid-dependent diffusivities, shear viscosity, bulk viscosity and thermal conductivity, respectively. High-wavenumber models for these coefficients, appropriate for Cartesian grids, are

$$D_\alpha = C_D \frac{\Delta^2}{\Delta t}\overline{\eta} \ , \quad \eta = \begin{cases} -Y_\alpha & \text{if } Y_\alpha < 0 \\ 0 & \text{if } 0 \le Y_\alpha \le 1 \\ Y_\alpha - 1 & \text{if } Y_\alpha > 1 \end{cases} \ , \tag{8}$$

$$\mu = C_\mu \overline{\rho \Delta^{r+1} S} \ , \quad S = (S_{ij}S_{ij})^{1/2} \ , \quad S_{ij} \equiv \frac{1}{2}\left(\frac{\partial^r u_i}{\partial x_j^r} + \frac{\partial^r u_j}{\partial x_i^r}\right) \ , \tag{9}$$

$$\mu_b = C_b \overline{\Delta^{r+1} B/c} \ , \quad B = (B_i B_i)^{1/2} \ , \quad B_i = \frac{\partial^r p}{\partial x_i^r} \ , \tag{10}$$

$$k = C_k \overline{c_p \rho \Delta^{r+1} Q^{1/2}} \ , \quad Q = (Q_i Q_i)^{1/2} \ , \quad Q_i = \frac{\partial^r e}{\partial x_i^r} \ , \tag{11}$$

where the overbar denotes a Gaussian filter. In practice, C_D is chosen to reduce overshoots and undershoots in the mass fractions, C_μ is tuned to reduce ringing in the vorticity field, C_b is adjusted to reduce Gibbs oscillations near shocks and C_k is selected to reduce ringing in temperature. The derivatives in (9), (10) and (11) provide a k^r weighting of the damping terms in Fourier space. Convergence rates of $\mathcal{O}(r)$ have been demonstrated in one-dimensional simulations of a breaking wave. Larger values of r lead to shaper truncation of the energy spectrum, and hence, a broader inertial range. For $r = 8$, the following sixth-order compact scheme has been found to work well for computing the derivatives,

$$29u_j^{VIII} + 14\left(u_{j+1}^{VIII} + u_{j-1}^{VIII}\right) + (3/2)\left(u_{j+2}^{VIII} + u_{j-2}^{VIII}\right)$$
$$= [4200u_j - 3360(u_{j+1} + u_{j-1}) + 1680(u_{j+2} + u_{j-2}) - 480(u_{j+3} + u_{j-3}) + 60(u_{j+4} + u_{j-4})]/\Delta^8 \ .$$

Large-eddy simulations have been conducted using these models in conjunction with 10th-order compact differencing and 4th-order Runge-Kutta timestepping. Superior results are obtained, compared to various MILES algorithms, on a variety of test cases, including Shu's problem, a breaking wave, the Taylor-Green vortex, Richtmyer-Meshkov instability and Rayleigh-Taylor instability.

This work was performed under the auspices of the U.S. Department of Energy by the University of California Lawrence Livermore National Laboratory under contract No. W-7405-Eng-48.

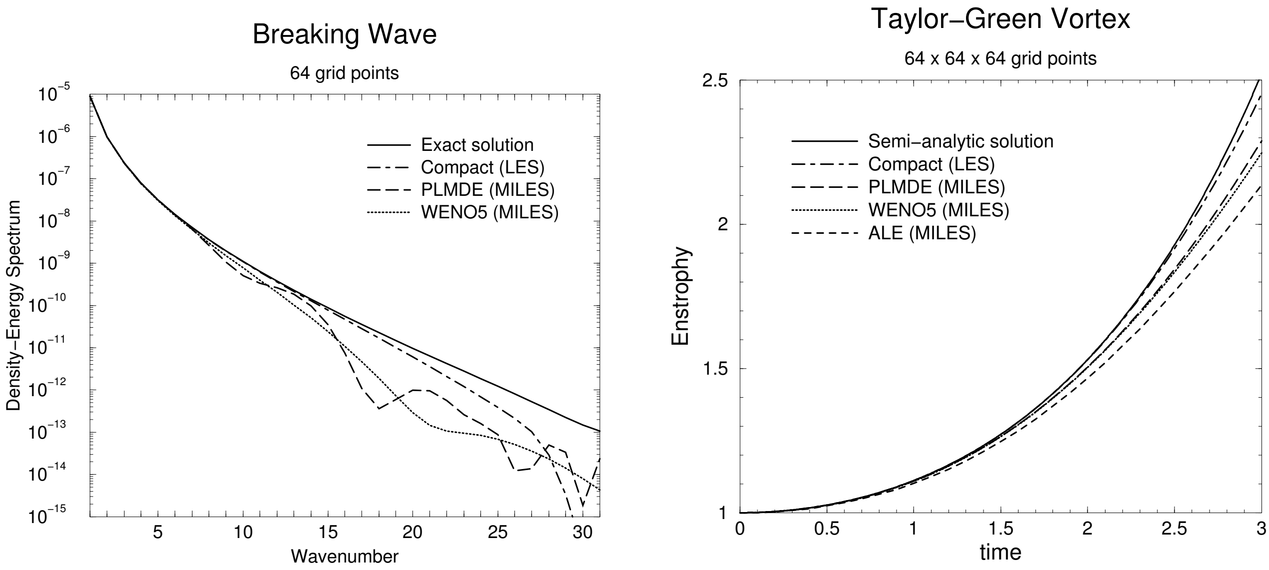

Figure 1: Comparisons of high-resolution (compact) LES method against standard MILES techniques. On the left is the density-energy spectrum of a compressible wave just prior to shock formation. On the right is normalized total enstrophy for the Taylor-Green vortex.

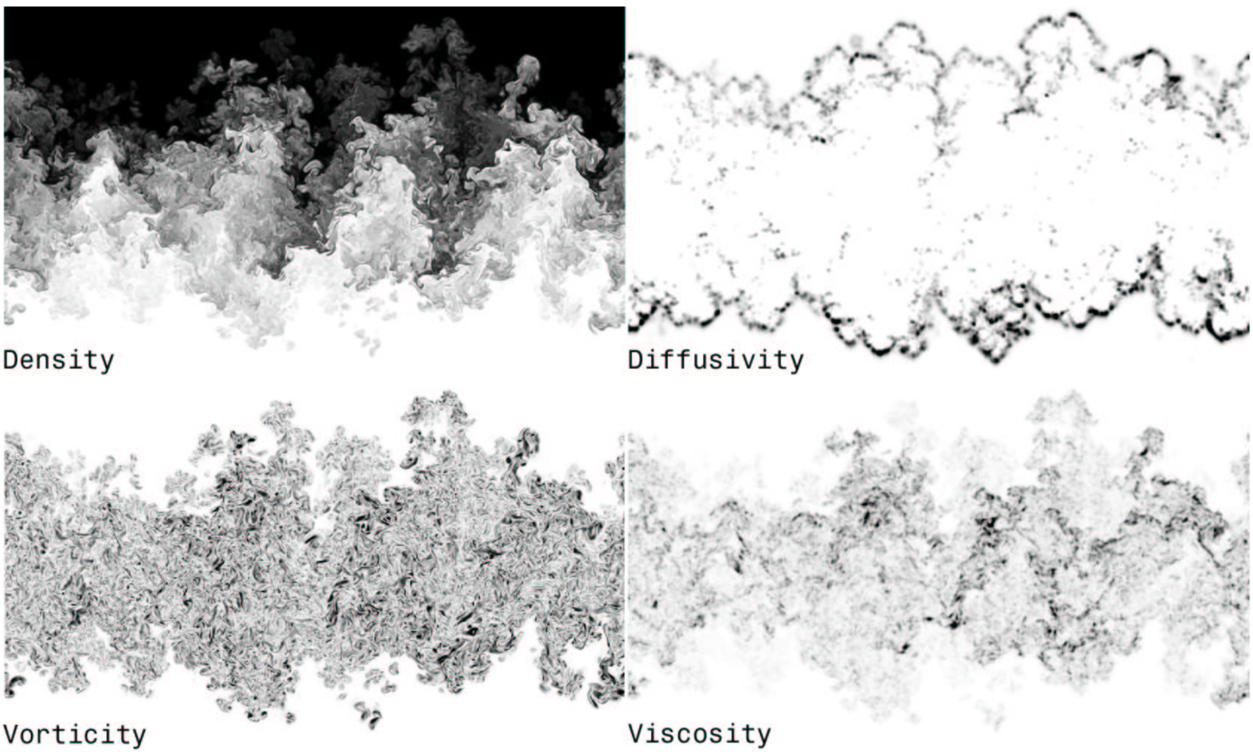

Figure 2: Side-on views of mixing region from 1152^3 point large-eddy simulation of Rayleigh-Taylor instability. Top left is density, top right is subgrid-scale diffusivity, bottom left is vorticity magnitude and bottom right is subgrid-scale viscosity.